Signal Processing and Renewable Energy
September 2021, (pp. 1-22)
ISSN: 2588-7327
eISSN: 2588-7335

Coexisting Behaviors Analysis and Chaos-Based Secure Communication Scheme by a Novel High-Order Nonlinear Autonomous System

Javad Mostafaee[1], Saleh Mobayen[1,2], Behrouz Vaseghi*[1,3], Mohammad Vahedi[1]

[1] Department of Electrical Engineering, Saveh Branch, Islamic Azad University, Saveh, Iran.
[2] Department of Electrical Engineering, University of Zanjan, Zanjan, Iran.
[3] Department of Electrical Engineering, Abhar Branch, Islamic Azad University, Abhar, Iran.

Received: 28-Dec-2020, Revised: 25-Feb-2021, Accepted: 28-Feb-2021.

Abstract

This paper constructs a new 6–D hyper–chaotic system with complex dynamic behaviors for secure communication scheme. We analyze the chaotic attractor, bifurcation diagram, equilibrium points, Poincare map, Lyapunov exponent behaviors, and Control parameter. The more nonlinear the autonomous system is and the higher the parametric sensitivity it is, the more performative it will be and the more difficult it will be to decode. We will show that the designed system will have attractive and different behaviors due to very small changes in control parameters, which is a sign of the high sensitivity of the system. Then, with the construction of master-slave systems and the design of a new terminal sliding mode controller, the application of the hyper-chaotic system in synchronization and transmission of secure communications is shown. Finally, using the MATLAB simulation, the results are confirmed for the new hyper–chaotic system.

Keywords: Chaotic Analysis, Nonlinear Autonomous System, Secure Communication Scheme, Terminal Sliding Mode Control, Finite-Time Synchronization.

1. INTRODUCTION

In recent years, communications and information technology systems have a special place and the secure communication of this information is very important.

Due to the existence of information networks in military structures, medicine, trade and other structure, increasing security has a special importance and place. Compared to traditional methods, information transfer using chaotic systems has some advantages such as speed, security

*Corresponding Authors Email: behrouz.vaseghi@gmail.com

and capability [1]. Chaotic systems have a number of intrinsic properties, including high–complex as well as nonlinear dynamical equations. Three key features of these systems are their high complexity, uncertainties in the system parameters, and extreme sensitivity to very small changes in their initial conditions [2]. Because of these features, these systems have been used in many fields, including image encryption [3], medical science [4], mechanics [5], space Science [6], control synchronization [7], physics [8] and secure communications [9]. In recent years, new chaotic systems have been introduced for secure communications [10-14]. These communication systems are less secure, due to the presence of only one positive Lyapunov exponents view compared to hyper-chaotic systems with two or more positive Lyapunov exponents views. The researchers found that the more complex and large the system is, the more secure it is in chaos-based secure communication [15]. There are two reasons: First, the low-dimensional the system is, the less band-width it has and the easier it can be separated by a filter. Second, high-order systems are more dynamic and complex than low-order systems and are more unpredictable. There are two main ideas for secure communication, one is control and the other is synchronization. These ideas were first proposed by Afraimovich' et al [16]. And later improved [17]. With the development of this idea [18-23], researchers have shown experimentally and theoretically that if two master-slave systems are synchronized, information transfer can be achieved. Dynamic systems synchronization is the power of two systems to track each other's behavior.

In order to transfer chaos-based secure communication, many hyper-chaotic systems have been developed, each with its own unique characteristics [24-27]. In [28], a six-dimensional hyper-chaotic system with four positive Lyapunov exponent's has been reported. Lyapunov exponent's is the average speed of two-point transmission paths in chaotic systems. The positive of this index shows the degree of divergence and its negative shows the degree of convergence of system states. Then, using phase portraits analysis, the high-pressure of the system has been proved. The results indicate the optimal performance of the system. In [29], by adding a dimension to the Lorenz hyper-chaotic system, a five-dimensional system is created that has three positive Lyapunov symbols. The existence of adsorbents in this system has been confirmed using Poincaré map. Then the electrical circuit is made suitable for this system. It has been proven that the system is very sensitive to changes in the initial conditions and parameters, which indicates the specificity of the system.

In recent years, various methods and controllers have been used to synchronize hyper-chaotic systems, including: output-feedback control [30], adaptive control [12], passive control [31], optimal control [32, 33], PID control [34], adaptive backstepping control [35], linear control [36], neural network [37], predictive control [38], stochastic control [39], backstepping design [40], sliding mode control [41-43] and terminal sliding mode control [44-46]. Between the stated methods, sliding mode control (SMC) has some special specs such

as: parametric uncertainties, robustness versus, simple implementation, suitable transient response, reduction of the order of the system, less sensitivity to bounded disturbance and computational simplicity [47]. Although SMC is very popular and efficient, but this method has a big drawback called chattering. In practice, chattering is a very undesirable phenomenon because it can increase energy consumption, cause mechanical wear in systems and actuators and deteriorate controller performance. Much research has been done to solve the problems of this method [48-50]. For example in [51] a new sliding mode control is used by combining PID and sling mode methods. The new controller is robust against disturbances and has no chattering and is able to provide convergence in a finite-time. In [52], robust sliding mode control without chattering is used to control and track a remote vehicle with three degrees of freedom in the presence of uncertainty. The new controller has been able to reduce chattering as much as possible in the presence of uncertainties and disturbances, while maintaining robustness and accurate tracking. In [53], a finite-time controller is used, using a neural network with uncertainty in the system. The cost function used includes continuous and intermittent feedback controllers. finite-time control is designed in accordance with the cost function that can provide convergence in limited time. The proposed controller was able to optimize the quadratic cost function and reduce convergence time. In conventional SMC algorithm, the most commonly used sliding variable is the linear which is based on linear combination of the system errors by using an appropriate coefficient. Instead of using a linear sliding variable, Terminal Sliding Mode Control (TSMC) with a nonlinear sliding variable is present. The terminal sliding mode was developed by adding the nonlinear fractional power item into the sliding variable in sliding phase to offer some superior properties, such as finite time convergence of state variables, faster and better tracking precision. Also, nonlinear sliding variable in TSMC can improve the transient performance statically.

This paper includes two main new structures, one is the use of a high-order nonlinear autonomous system and the other is the use of a fast controller that provides safe data transmission in the finite-time. These structures can be classified as follows:

- A novel 6-D hyper-chaotic system has been constructed to increase communication security.
- The standard analysis of the new system has been performed and the sensitivity of the system has been discussed.
- A new TSMC controller has been designed and stabilized using the Lyapunov stability method.
- The synchronization technique is performed by entering an uncertainty in the system to secure communication in the finite-time.
- A comparison has been made between a new controller and a similar controller.

The rest of this paper is organized as follows: Sect. **2**, Introduction of a new 6-D hyper-chaotic system. In Sect. **3**, Standard analysis of the introduced system has been performed. In Sect. **4**, Chaos-based secure communication scheme and simulation

results are given to demonstrate the efficiency and advantages of the suggested method. Finally, we end this paper with some conclusions in Sect. **5**.

2. INTRODUCTION OF A NEW 6-D HYPER-CHAOTIC SYSTEM

The new 6-D hyper-chaotic system designed by the following equations is introduced as follows:

$$\begin{aligned} dx(\tau)/d(\tau) &= a_1(y-x)-a_2v \\ dy(\tau)/d(\tau) &= a_3x-a_4u-y-xz \\ dz(\tau)/d(\tau) &= -a_5z+xy+x^2 \\ du(\tau)/d(\tau) &= a_6(y+v)+w+kyz \\ dv(\tau)/d(\tau) &= a_7y+x-w \\ dw(\tau)/d(\tau) &= -a_8x+a_9u-v \end{aligned} \quad (1)$$

where $(x,y,z,u,v,w)^T \in \Re^6$ are state variables and $a_1,...,a_9 \in \Re$ are parameters and $k \in \Re$ is hyper-chaos control parameter. With parameters:

$$\begin{aligned} &a_1=13.47,\ a_2=0.85,\ a_3=37.2, \\ &a_4=19.41,\ a_5=8.13, a_6=2.92, \\ &a_7=5.17,\ a_8=4.32,\ a_9=0.54,\ k=0 \end{aligned} \quad (2)$$

and initial conditions:

$$\begin{aligned} &x_0(\tau)=-0.4,\ y_0(\tau)=1.6,\ z_0(\tau)=-4.05, \\ &u_0(\tau)=2.7,\ v_0(\tau)=-1.8,\ w_0(\tau)=0.2 \end{aligned} \quad (3)$$

System (1) has hyper-chaotic behaviors. The system (1) divergence is as follows:

$$\begin{aligned} \nabla V = \sum_{\iota=1}^{6} \frac{\partial \dot{x}_\iota}{\partial x_\iota} = -a_1-1-a_5+0+0+0= \\ -13.47-1-8.13=-22.6<0 \end{aligned} \quad (4)$$

.

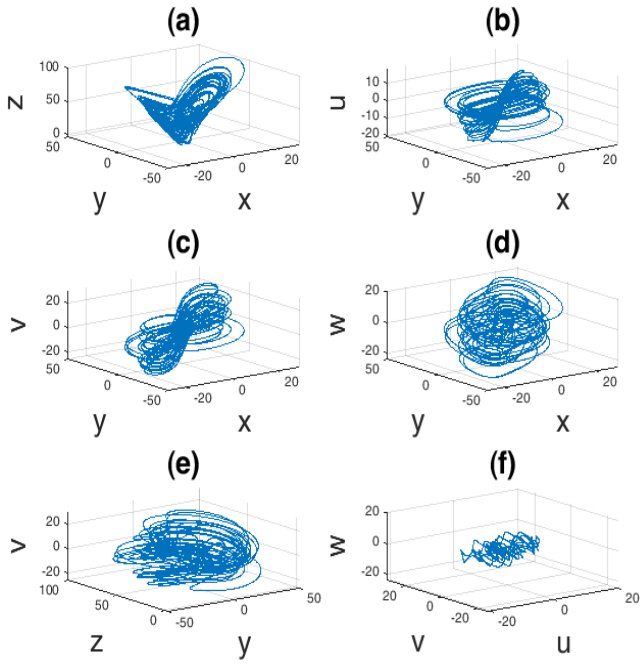

Fig. 1. Analysis of chaotic absorbers of system (1) in (a) $x-y$ plane, (b) $x-z$ plane, (c) $y-z$ plane, (d) $x-w$ plane, (e) $x-y-z$ plane and (f) $x-y-v$ plane.

The convergence speed of the system (1) to its attractors is $e^{-(-a_1-1-a_5)\tau}$ at time τ. Therefore, the system paths converge to the origin and the system will eventually remain motionless on its absorbers. the 3-D phase portrait diagrams of the system (1) with parameters (2) and initial conditions (3) is shown in Fig. 1

3. PROPERTIES OF THE HYPER-CHAOTIC MODEL

In this section, we will review and analyze common methods in evaluating the performance of chaotic systems and introduce the characteristics of the new hyper-chaotic system (1). In the simulations we use the Runge–Kutta method and consider the time step equal to $\Delta(\tau) = 0.001$. In the following, we will examine the type of system behavior with two important methods of qualitative analysis of bifurcation diagrams (B.D.s) and quantitative analysis of Lyapunov exponents (L.E.s).

3.1. Stability and Equilibria

By setting the differential equations in (1) to zero, it is concluded that the new system (1) has equilibrium point at: $Q = (0,0,0,0,0,0)$. When the parameter values are considered as in (1), the system linearization matrix [54] at the equilibrium point Q is given by

$$J = \frac{\partial F_i}{\partial x_j}(x)\Big|_{Q^*} = \begin{bmatrix} -a_1 & a_1 & 0 & 0 & -a_2 & 0 \\ a_3 & -1 & 0 & -a_4 & 0 & 0 \\ 0 & 0 & -a_5 & 0 & 0 & 0 \\ 0 & a_6 & 0 & 0 & a_6 & 1 \\ 1 & a_7 & 0 & 0 & 0 & -1 \\ -a_8 & 0 & 0 & a_9 & -1 & 0 \end{bmatrix} \quad (5)$$

According to (5), the system eigenvalues are found as follows: $\rho(s) = \left|sI_d - J\right| = 0$ with I_d, as an 6×6 identity matrix. That is

$$\lambda_1 s^5 + \lambda_2 s^4 + \lambda_3 s^3 + \lambda_4 s^2 + \lambda_5 s + \lambda_6 = \Delta(s) \quad (6)$$

Using parameter values in (2), the eigenvalues are $s_1 = -30.0247$, $s_2 = 11.3098$, $s_3 = -8.13$, $s_4 = 6.2926$, $s_5 = -1.9024$, $s_6 = -0.1453$. Thus, Q is an unstable saddle.

3.2. Chaotic Analysis

To investigate the dependence of the parameters of the new hyper–chaotic system (1), we need to draw and analyze the bifurcation diagram. In Fig. 2 the bifurcation diagrams of new hyper-chaotic system are plotted. The system enters into chaotic oscillations with routine period doubling [55].

As an interesting method, we used the Poincaré map to describe the folding attributes of the chaotic system. To study the performance and behavior of continuous dynamical systems, similar to the proposed system (1), we can use the Poincaré map, one of the most popular topics in nonlinear dynamic analysis. Figure 3 displays a 2-D Poincaré map of system (1) with a related phase portrait. As it is known, the Poincaré map of the hyper-chaotic system corresponds to the phase portrait of the system [56, 57]. According to Fig. 3, the regular set of points depicted in the Poincare maps is an indication of the system's chaotic behavior.

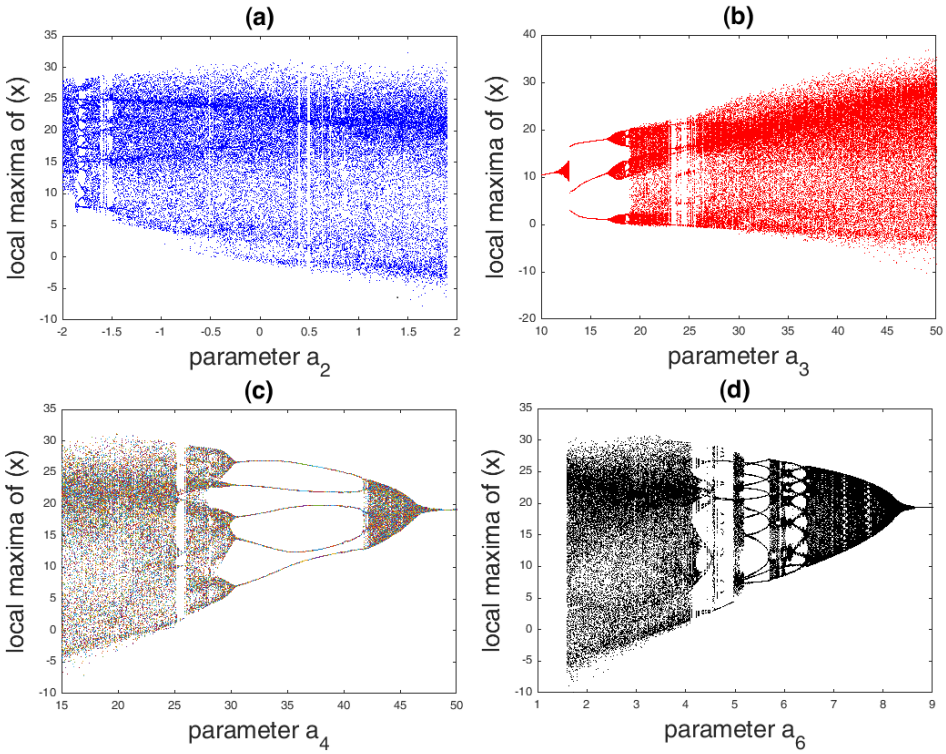

Fig. 2. Bifurcation diagrams with initial conditions (3) and changes made in the parameters of (2) and changes in (a) parameter a2, (b) parameter a3, (c) parameter a4 and (d) parameter a6.

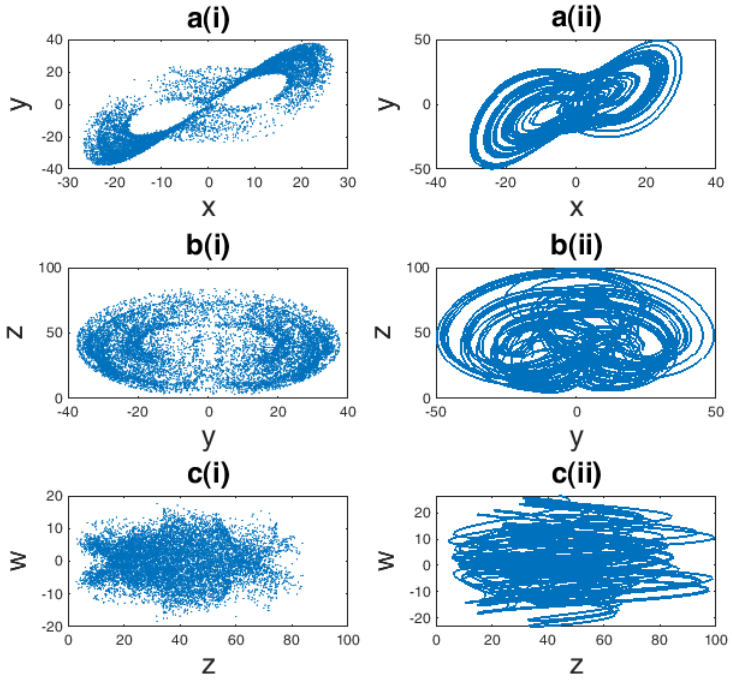

Fig. 3. Poincaré map (i) and 2–D phase portrait (ii) of the system (1) in (a) x–y space, (b) y-z space and (c) z–w space.

The divergence and convergence of the states of a nonlinear system are determined by its L.E.s' representation. If L.E.s are positive, it indicates the chaotic behavior of the system [58]. A system is hyper–chaotic if there are two or more positive L.E.s. The L.E.s of the exponential hyper–chaotic system (1) using Wolf's algorithm [58] with different initial conditions (3) and parameters (2) are numerically found as L.E1=0.89308, L.E2=0.10658, L.E3=0, L.E4=-1.41338, L.E5=0, L.E6=0 shown in Fig. .

Another characteristic of the chaotic systems, is the sensitivity to change in the initial conditions. Fig. display the 2–D phase portraits of the novel hyper–chaotic system (1) with parameters (2) and three different initial conditions.

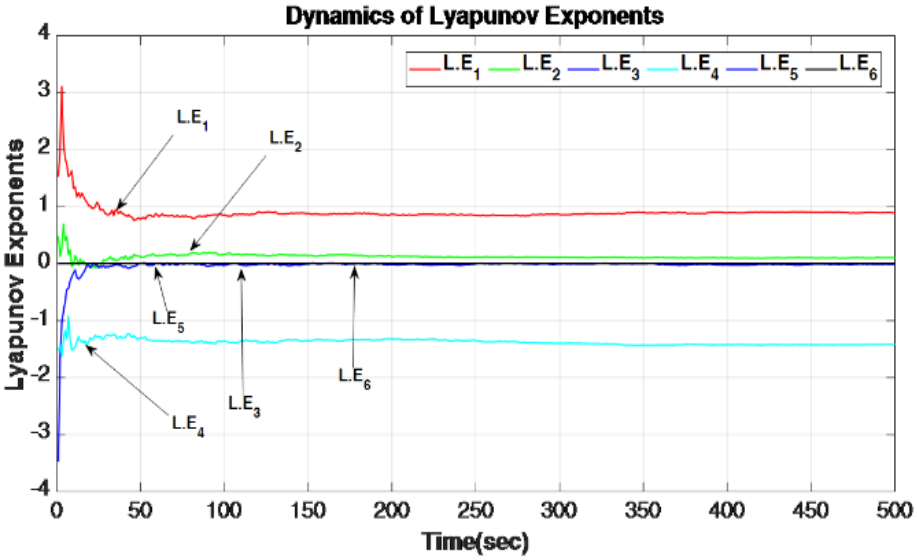

Fig. 4. Dynamics L.E.s of the novel six–dimensional system (1) with parameters (2) and initial conditions (3).

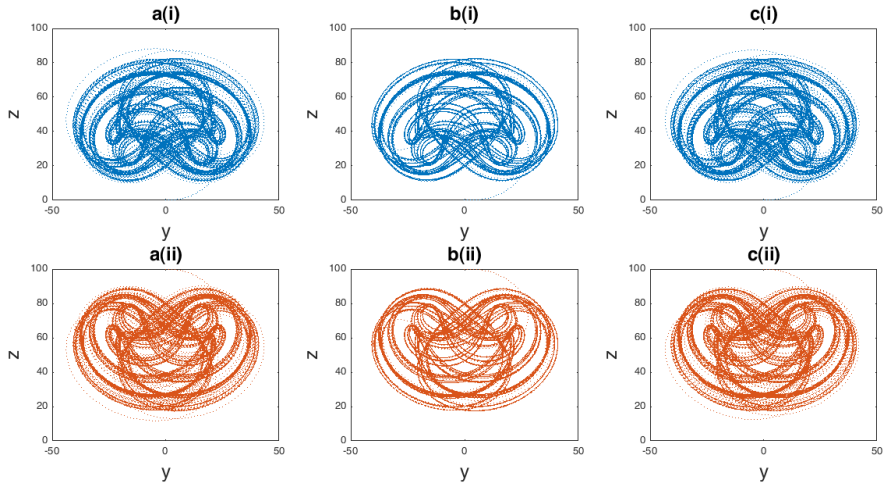

Fig. 5. The phase portrait diagrams of the system (1) on the $y-z$ space with parameters (2) for three different initial conditions: (a) [–0.01, –0.1, –0.01, –0.1, –0.01, –2.5], (b) [–0.1, –0.1, –0.1, –2.5, –0.1, –0.1] and (c) [–0.1, –0.1, –0.1, –0.1, –0.1, –2.5].

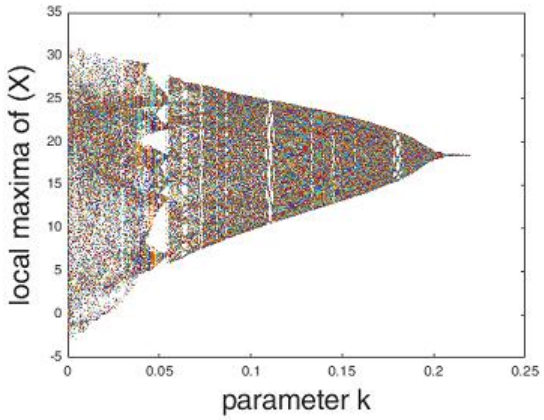

Fig. 6. Bifurcation diagram (B.D.s) of the system (1) with local maxima of x and control parameter $k \in [0,0.25]$.

3.3. Chaos and Hyper-Chaos

System (1) is assumed with the initial conditions (3), control parameter k and parameters (2). Fig. display the Bifurcation diagram (B.D.s) of a designed hyper-chaotic system in $k \in [0,0.25]$. In this figure, we see the overlap of the curves with different colors, which is the hysteresis of the system [59]. Variation in the control parameter k, allows us to obtain several different adsorbents in $k \in [0,1.5]$.

When the control parameter k is in this range, the system will have complex behaviors such as hyper-chaotic, chaotic, periodic and quasi-periodic. These behavioral changes are shown in Fig. , proportion to L.E.s changes. Dynamic behaviors of the system (1) with changes in k include the following:

I. When $k \in (0, 0.05]$, the L.E.s of system (1) at $k = 0.04$ are (0.30668, 0.00376, -0.034823, -1.52462, 0, 0). In this case, the system (1) has a hyper-chaotic behavior and the 1-D and 3-D phase portraits are shown in Fig. (a).

Table 1. ***L.E.s and complex dynamical behavior with different control parameter k.***

Parameter k	(L.E1, L.E2, L.E3, L.E4, L.E5, L.E6)	Dynamic behaviors
(0, 0.05]	(+, +, –, –, 0, 0)	Hyper-chaotic
(0.05, 0.15]	(+, –, –, –, 0, 0)	chaotic
(0.15, 0.25]	(+, –, –, –, 0, 0)	chaotic
(0.25, 0.5]	(0, –, –, –, 0, 0)	periodic
[1, 1.5)	(0, 0, –, –, 0, 0)	Quasi-periodic

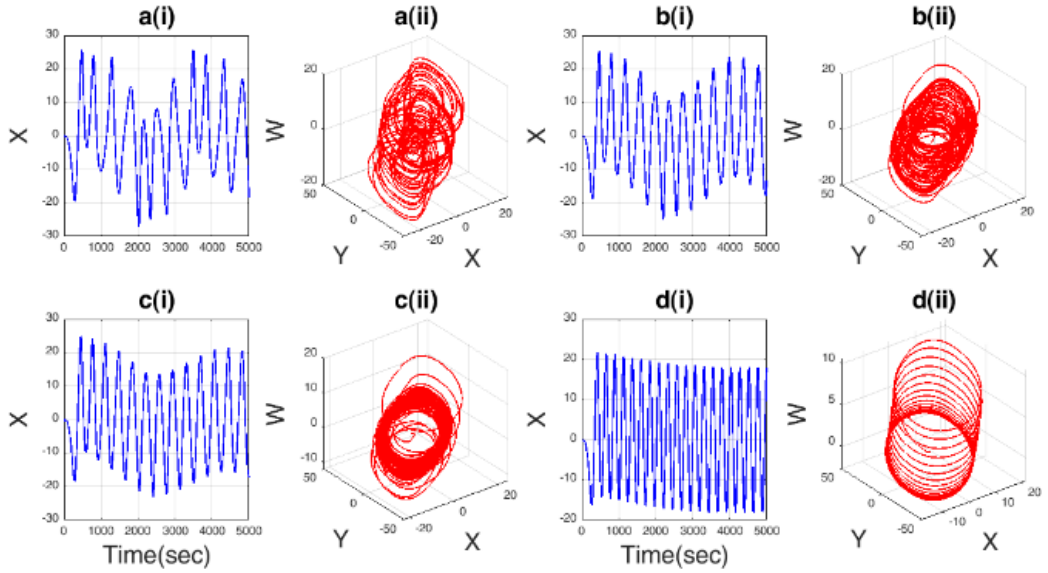

Fig. 7. 1-D time series (i) and 3-D phase portrait (ii) of system (1) with initial condition (3) and changing the control parameter k in (a) k=0.04, (b) k=0.13, (c) k=0.2 and (d) k=0.77.

II. When $k \in (0.05, 0.15]$, the L.E.s of system (1) at $k = 0.13$ are (0.00664, -0.00405, -0.86748, -1.11307, 0, 0). In this case, the system (1) has a chaotic behavior and the 1-D and 3-D phase portraits are shown in Fig. (b).

III. When $k \in (0.15, 0.25]$, the L.E.s of system (1) at $k = 0.2$ are (0.00718, -0.01938, -0.0294, -0.95119, 0, 0). In this case, the system (1) has a chaotic behavior and the 1-D and 3-D phase portraits are shown in Fig. (c).

IV. When $k \in (0.25, 0.5]$ and $k \in [1,1.5)$, the L.E.s of system (1) at $k = 0.77$ are (0, -0.53618, -1.32396, -1.33496, 0, 0). In this case, the system (1) has a periodic behavior and the 1-D and 3-D phase portraits are shown in Fig. (d).

4. SYNCHRONIZATION

4.1. Terminal Sliding Model Control Design

Consider the following system:

$$\dot{\mathrm{X}}(\tau) = \Gamma \mathrm{X}(\tau) + \mathrm{B}\upsilon(\tau) + \xi(\mathrm{X}(\tau)) + D(\tau) \tag{7}$$

where $\mathrm{X}(\tau) \in \Re^{n\times 1}$ is the system state variable, $\Gamma \in \Re^{n\times n}$ and $\mathrm{B} \in \Re^{n\times 1}$ are the constant matrices, $\upsilon(\tau) \in \Re^{n\times 1}$ is the controller, $\xi(\mathrm{X}(\tau)) \in \Re^{n\times 1}$ is the nonlinear function of the system and $D(\tau) \in \Re^{n\times 1}$ is the unknown disturbance of the system.

Assumption 1: Γ, B and $\xi(\mathrm{X}(\tau))$ which are nonlinear functions, change over time.

The sliding surface for System (7) is described as:

$$\delta(\mathrm{X}(\tau)) = \zeta \mathrm{X}(\tau) + (\int_0^{\tau} \Psi(\mathrm{X}(t))dt) \\ (\left\|\mathrm{X}(\tau)\right\| + \left\|\mathrm{X}(\tau)\right\|^{\gamma}) \tag{8}$$

where ζ and γ signify the positive constant vajlues of the system, and $\Psi(\mathrm{X}(t)) = \dfrac{\mathrm{X}_i(t)}{\left\|\mathrm{X}_i(t)\right\|}$

Theorem 1: Consider the disturbed dynamic system (7). Let the fast terminal sliding controller FTSMC is defined as:

$$\begin{aligned}\vartheta(\tau) &= \frac{\delta(\mathrm{X}(\tau))}{\left\|\delta(\mathrm{X}(\tau))\right\|^2 + \varepsilon} \\ &\left[\frac{G}{\eta}(-\xi(\mathrm{X}(\tau)) - \Gamma\mathrm{X}(\tau) + \lambda\mathrm{X}(\tau)) - \frac{1}{\zeta\eta}\Psi(\mathrm{X}(\tau))\right. \\ &\left.(\left\|\mathrm{X}(\tau)\right\| + \left\|\mathrm{X}(\tau)\right\|^{\gamma}) - \frac{\rho}{\zeta\eta}\right]\left\|\delta(\mathrm{X}(\tau))\right\| \\ &+ \chi\tanh^2(\delta(\mathrm{X}(\tau)))\end{aligned} \tag{9}$$

where $\varepsilon,\ \eta, \lambda$ and G are optional positive constants and χ is a scalar value which satisfies

$$\chi = \sup\left(G\left(\frac{\xi(\mathrm{X}(\tau))}{\eta} + D(\tau) + \dot{D}(\tau)\right)\right) \tag{10}$$

Then, the states of the dynamical system (7) move to the sliding surface (8) in the finite–time and remain on it.

Proof: The Lyapunov candidate function can be considered as follows:

$$\omega(\tau) = 0.5\delta(\mathrm{X}(\tau))^T\delta(\mathrm{X}(\tau)) \tag{11}$$

According to TSMC theory, the sliding surface and its derivative to reach the slippery surface must be $\delta(\mathrm{X}(\tau)) = 0$ and $\dot{\delta}(\mathrm{X}(\tau)) = 0.$ Therefore, by deriving Equation (8), we will have:

$$\dot{\delta}(\mathrm{X}(\tau)) = \zeta\dot{\mathrm{X}}(\tau) + \Psi(\mathrm{X}(\tau))(\left\|\mathrm{X}(\tau)\right\| + \left\|\mathrm{X}(\tau)\right\|^{\gamma}) \tag{12}$$

Substituting the (7) in (12), we will have

$$\begin{aligned}\dot{\delta}(\mathrm{X}(\tau)) &= \zeta\left[\xi(\mathrm{X}(\tau)) + \Gamma\mathrm{X}(\tau) + \upsilon(\tau)\right] \\ &+ \Psi(\mathrm{X}(\tau))(\left\|\mathrm{X}(\tau)\right\| + \left\|\mathrm{X}(\tau)\right\|^{\gamma})\end{aligned} \tag{13}$$

Taking the derivative of the Lyapunov candidate (11) and substituting FTSMC (9) into the system (7), we will have

$$\begin{aligned}\dot{\omega}(\tau) &= \delta^T(\mathrm{X}(\tau))\dot{\delta}(\mathrm{X}(\tau)) \\ &= \delta^T(\mathrm{X}(\tau))\begin{bmatrix}\zeta\dot{\mathrm{X}}(\tau) + \Psi(\mathrm{X}(\tau)) \\ (\left\|\mathrm{X}(\tau)\right\| + \left\|\mathrm{X}(\tau)\right\|^{\gamma})\end{bmatrix} \\ &= \delta^T(\mathrm{X}(\tau))\begin{bmatrix}\zeta\xi(\mathrm{X}(\tau)) + \Gamma(\mathrm{X}(\tau)) \\ +\upsilon(\tau) + \Psi(\mathrm{X}(\tau)) \\ (\left\|\mathrm{X}(\tau)\right\| + \left\|\mathrm{X}(\tau)\right\|^{\gamma})\end{bmatrix} \\ &= \delta^T(\mathrm{X}(\tau))\left[\zeta\begin{pmatrix}\xi(\mathrm{X}(\tau)) + \Gamma(\mathrm{X}(\tau)) \\ -\lambda\mathrm{X}(\tau) + \eta\Psi(\mathrm{X}(\tau))\end{pmatrix}\right. \\ &\left. + \Psi(\mathrm{X}(\tau))(\left\|\mathrm{X}(\tau)\right\| + \left\|\mathrm{X}(\tau)\right\|^{\gamma})\right]\end{aligned} \tag{14}$$

Using (9) and (14), we obtain:

$$\begin{aligned}\dot{\omega} &\le -\rho\left\|\delta(\mathrm{X}(\tau))\right\| - \left\|\delta(\mathrm{X}(\tau))\right\|^{\gamma+1} \\ &\le \bar{\rho}\omega^{0.5}(\tau) - \beta\omega^{\alpha}\end{aligned} \tag{15}$$

where $\bar{\rho} = \sqrt{2}\rho$, $\beta = 2^{\alpha}$ and $\alpha = (\gamma+1)/2.$

Equation (15) shows that, the Lyapunov function (11) is decreased gradually and the sliding surface converges to origin in the finite–time. So, this completes the proof.

4.2. Disturbance Formulation

Assumption 2: In general, consider the constraints on the disturbance and uncertainty as

$$\left|F(\mathrm{X}(\tau))\right| \le \gamma_1 \,,\ \left|D(\tau)\right| \le \gamma_2 \tag{16}$$

where γ_1 and γ_2 denote positive unknown constants.

***Definition 1**:* To prove the efficiency of the controller, we consider the disturbance term as follows:

$$D(\tau) = \begin{bmatrix} d_1(\tau) \\ d_2(\tau) \\ d_3(\tau) \\ d_4(\tau) \\ d_5(\tau) \\ d_6(\tau) \end{bmatrix} = \begin{bmatrix} 0.1\sin(20t)+18 \\ -0.3\cos(30t)+1.5 \\ -1.5\sin(12t)+3.2 \\ 2\cos(14t)-7.2 \\ 6\sin(24t)-12 \\ 7\cos(9t)+4.7 \end{bmatrix} \tag{17}$$

The hyper-chaotic system (1) by entering perturbation (17) as:

$$\begin{aligned} dx(\tau)/d\tau &= a_1(y-x) - a_2 v + 0.1\sin(20t) + 18 \\ dy(\tau)/d\tau &= a_3 x - a_4 u - y - xz - 0.3\cos(30t) + 1.5 \\ dz(\tau)/d\tau &= -a_5 z + xy + x^2 - 1.5\sin(12t) + 3.2 \\ du(\tau)/d\tau &= a_6(y+v) + w + kyz + 2\cos(14t) - 12 \\ dv(\tau)/d\tau &= a_7 y + x - w + 6\sin(24t) - 12 \\ dw(\tau)/d\tau &= -a_8 x + a_9 u - v + 7\cos(9t) + 4.7 \end{aligned} \tag{18}$$

Fig. display the 3-D phase portraits system (18) in the presence of disturbance. As it is known, compared to Fig. , the system has undergone many fluctuations and changes.

4.3. Finite-Time Synchronization Formulation

To achieve secure communication transmission, we need to design the master-

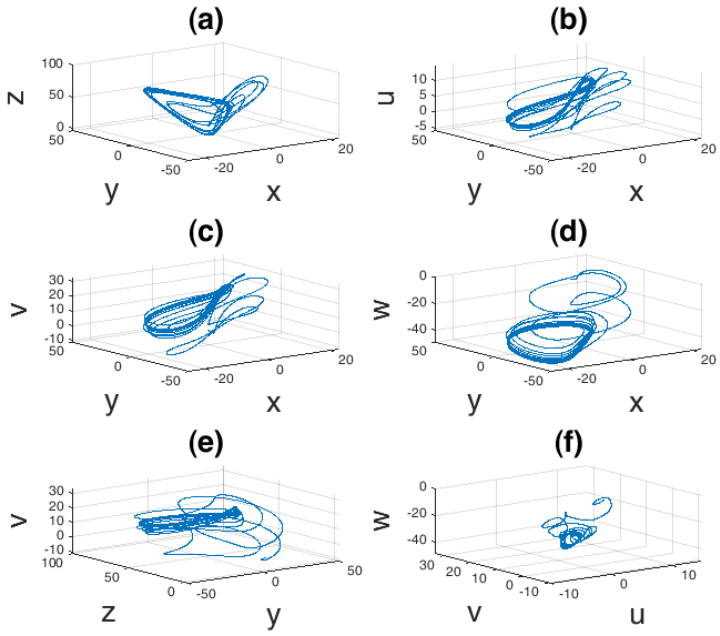

Fig. 8. 3-D phase portrait system (18) with disturbance in (a) x-y-z space, (b) x-y-u space, (c) x-y-v space, (d) x-y-w space, (e) y-z-v space and (f) u-v-w space.

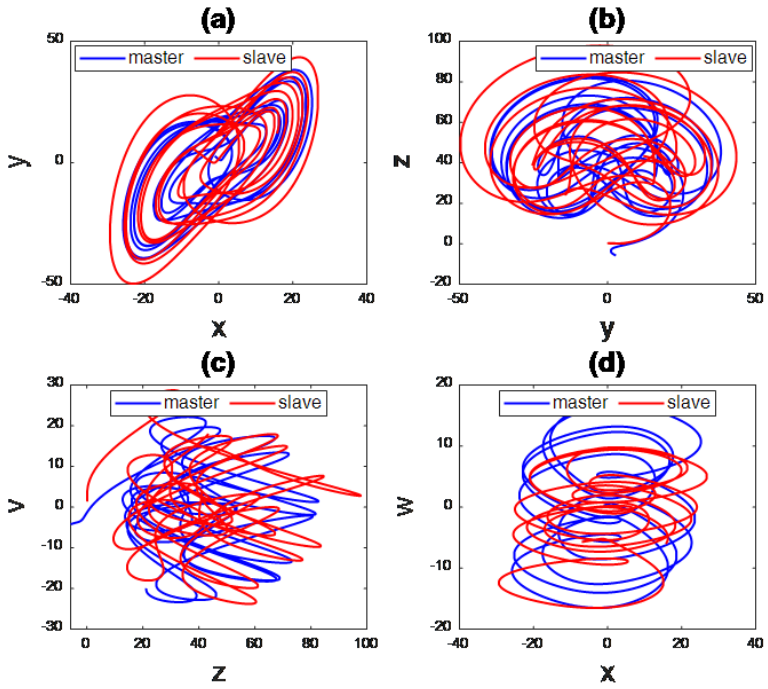

Fig. 9. 2-D phase portrait of master-slave systems in (a) x-y plane, (b) y-z plane, (c) z-v plane and (d) x-w plane.

slave systems. The master system is selected according to the main system (1) as follows:

$$\begin{aligned} dx_m(\tau)/d(\tau) &= a_{1m}(y_m - x_m) - a_{2m}v_m \\ dy_m(\tau)/d(\tau) &= a_{3m}x_m - a_{4m}u_m - y_m - x_m z_m \\ dz_m(\tau)/d(\tau) &= -a_{5m}z_m + x_m y_m + x_m{}^2 \\ du_m(\tau)/d(\tau) &= a_{6m}(y_m + v_m) + w_m + k_m y_m z_m \\ dv_m(\tau)/d(\tau) &= a_{7m}y_m + x_m - w_m \\ dw_m(\tau)/d(\tau) &= -a_{8m}x_m + a_{9m}u_m - v_m \end{aligned} \quad (19)$$

with parameters as follows

$$\begin{aligned} &a_{1m} = 13.47,\ a_{2m} = 0.85,\ a_{3m} = 37.2, \\ &a_{4m} = 19.41,\ a_{5m} = 8.13, \\ &a_{6m} = 2.92,\ a_{7m} = 5.17, \\ &a_{8m} = 4.32,\ a_{9m} = 0.54,\ k_m = 0.01 \end{aligned} \quad (20)$$

And initial conditions

$$\begin{aligned} &x_{0m}(\tau) = -1.06,\ y_{0m}(\tau) = 2.8, \\ &z_{0m}(\tau) = -5.75,\ u_{0m}(\tau) = 1.4, \\ &v_{0m}(\tau) = -4.2,\ w_{0m}(\tau) = 0.3 \end{aligned} \quad (21)$$

Similarly, for the slave system, we will have

$$\begin{aligned} dx_s(\tau)/d(\tau) &= a_{1s}(y_s - x_s) - a_{2s}v_s \\ dy_s(\tau)/d(\tau) &= a_{3s}x_s - a_{4s}u_s - y_s - x_s z_s \\ dz_s(\tau)/d(\tau) &= -a_{5s}z_s + x_s y_s + x_s{}^2 \\ du_s(\tau)/d(\tau) &= a_{6s}(y_s + v_s) + w_s + k_s y_s z_s \\ dv_s(\tau)/d(\tau) &= a_{7s}y_s + x_s - w_s \\ dw_s(\tau)/d(\tau) &= -a_{8s}x_s + a_{9s}u_s - v_s \end{aligned} \quad (22)$$

with parameters as follows

$$\begin{aligned} &a_{1s} = 13,\ a_{2s} = 0.95,\ a_{3s} = 37,\ a_{4s} = 19, \\ &a_{5s} = 8, a_{6s} = 3.5,\ a_{7s} = 6,\ a_{8s} = 3, \\ &a_{9s} = 0.6,\ k_s = 0.049 \end{aligned} \quad (23)$$

And initial conditions

$$\begin{aligned} &x_{0s}(\tau) = -7,\ y_{0s}(\tau) = 6,\ z_{0s}(\tau) = 0.1, \\ &u_{0s}(\tau) = -3.3, v_{0s}(\tau) = 1.4,\ w_{0s}(\tau) = -5.7 \end{aligned} \tag{24}$$

The two-dimensional phase diagram of master-slave systems with different initial conditions and parameters is shown in Fig. 9. As you can see, the two systems behave differently and must be synchronized to transfer secure communication.

Definition 2. The master system (19) with parameters (20) and initial conditions (21) and slave system (22) with parameters (23) and initial conditions (24) can be synchronized in a limited time τ [60].

$$\lim_{t\to\tau} \| X_{js} - X_{jm} \| = 0,\ \ j=1,2,...,N \tag{25}$$

Assumption 3: Suppose $y_i(\tau) = x_i(\tau)$ implies that $\lim_{\tau\to\infty} e_i(\tau) = 0$.

Assumption 4: Let the synchronization and finite–time synchronization errors of System (19) and System (22) be as: $e_i = x_{is} - x_{im}$ (i=1,...,6).

Based on Assumption 4, to study chaos synchronization, the error according to Systems (9) and (11) can be designed as follows

$$e_i = \sum_{i=1}^{4} y_i - x_i \Rightarrow \begin{pmatrix} \dot{e}_1(\tau) \\ \dot{e}_2(\tau) \\ \dot{e}_3(\tau) \\ \dot{e}_4(\tau) \\ \dot{e}_5(\tau) \\ \dot{e}_6(\tau) \end{pmatrix} = \begin{pmatrix} -a_1 e_1 + a_1 e_2 - a_2 e_5 \\ a_3 e_3 - e_2 - a_4 e_4 - x_s z_s + x_m z_m \\ -a_5 e_3 + x_s y_s - x_m y_m + x_s^2 - x_m^2 \\ a_6 e_2 + a_6 e_5 + e_6 + k y_s z_s - k y_m z_m \\ a_7 e_2 - e_1 - e_6 \\ -a_8 e_1 + a_9 e_4 - e_5 \end{pmatrix} \tag{26}$$

According to system (7), system (26) can be written in matrix form

$$\begin{pmatrix} \dot{e}_1(\tau) \\ \dot{e}_2(\tau) \\ \dot{e}_3(\tau) \\ \dot{e}_4(\tau) \\ \dot{e}_5(\tau) \\ \dot{e}_6(\tau) \end{pmatrix} = \begin{pmatrix} -a_1 & a_1 & 0 & 0 & -a_2 & 0 \\ 0 & -1 & a_3 & -a_4 & 0 & 0 \\ 0 & 0 & -a_5 & 0 & 0 & 0 \\ 0 & a_6 & 0 & 0 & a_6 & 1 \\ -1 & a_7 & 0 & 0 & 0 & -1 \\ -a_8 & 0 & 0 & a_9 & -1 & 0 \end{pmatrix} \begin{pmatrix} e_1(\tau) \\ e_2(\tau) \\ e_3(\tau) \\ e_4(\tau) \\ e_5(\tau) \\ e_6(\tau) \end{pmatrix} + \begin{pmatrix} 1 \\ 0 \\ 1 \\ 1 \\ 1 \\ 0 \end{pmatrix} u(\tau) + \begin{pmatrix} 0 \\ x_m z_m - x_s z_s \\ -x_m y_m - x_m^2 + x_s y_s + x_s^2 \\ -k y_m z_m + k y_s z_s \\ 0 \\ 0 \end{pmatrix} + \begin{pmatrix} 0.1\sin(20t) + 18 \\ -0.3\cos(30t) + 1.5 \\ -1.5\sin(12t) + 3.2 \\ 2\cos(14t) - 7.2 \\ 6\sin(24t) - 12 \\ 7\cos(9t) + 4.7 \end{pmatrix} \tag{27}$$

Definition 3. For chaos-based secure communication scheme, master system (19) and slave system (22) are synchronized in the finite-time using TSMC Controller (9).

Fig. and Fig. 3 displays the complete hyper–chaos synchronization of System (19) and (22). According to the error Equation

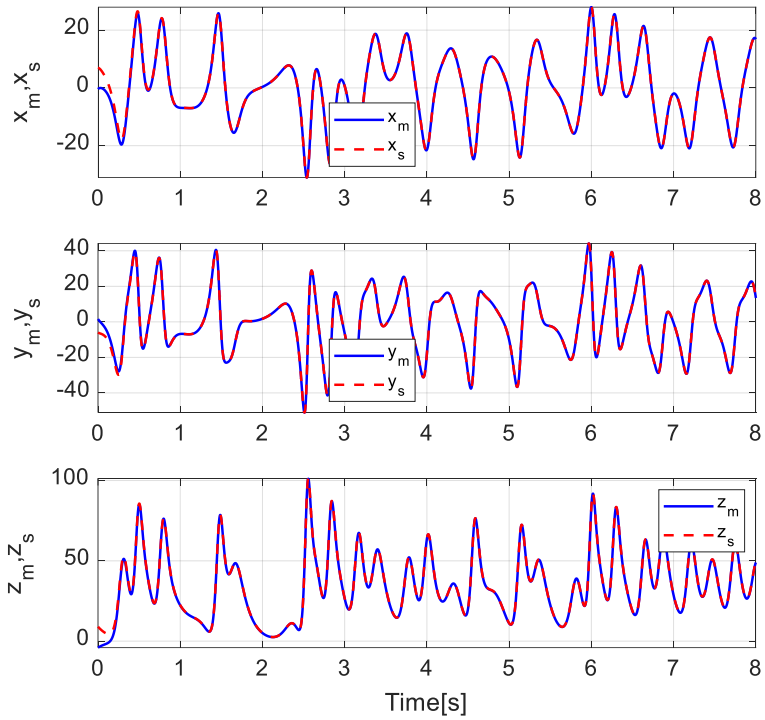

Fig. 10. Synchronization between two master–slave systems in x-y-z states.

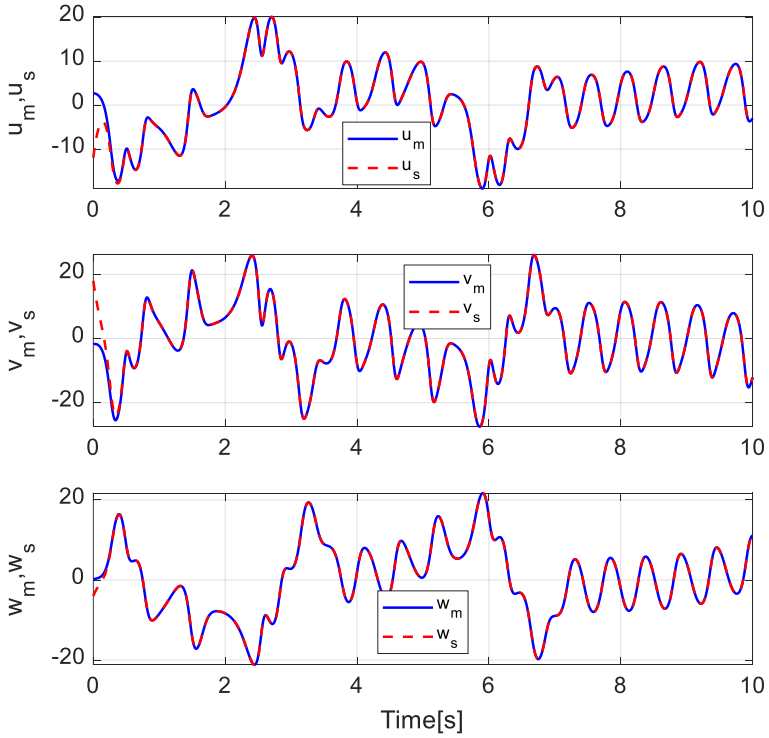

Fig. 3. Synchronization between two master–slave systems in u-v-w states.

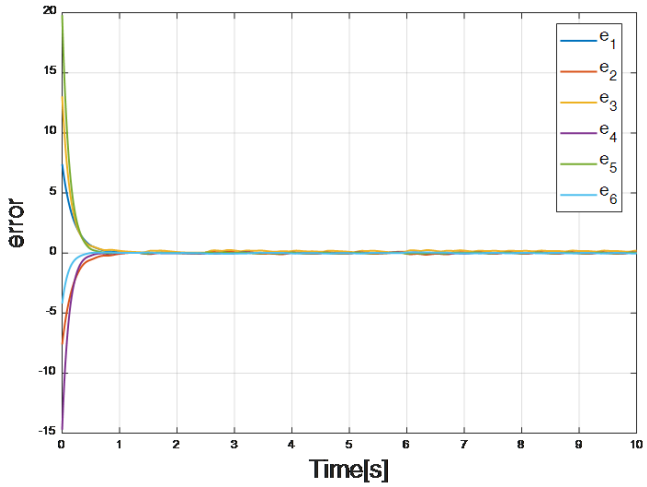

Fig. 4. The errors of synchronization with the controller

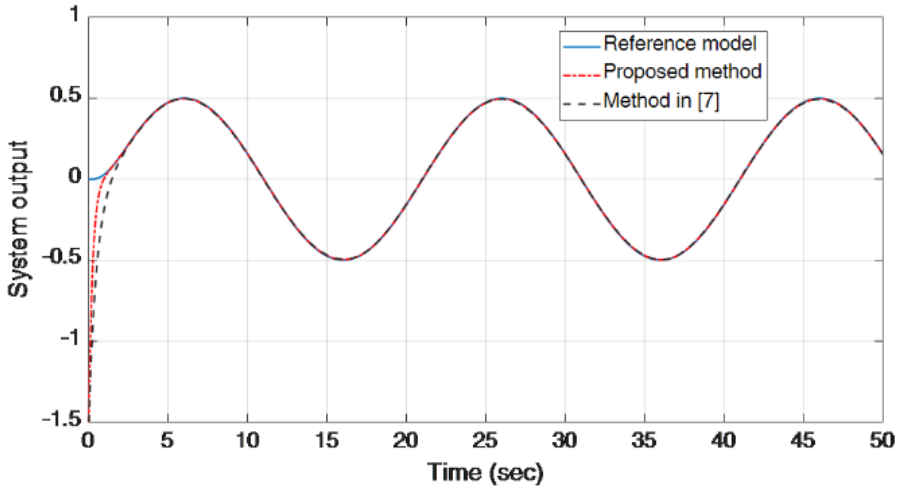

Fig. 5. Comparison of controllers in the presence of a reference signal.

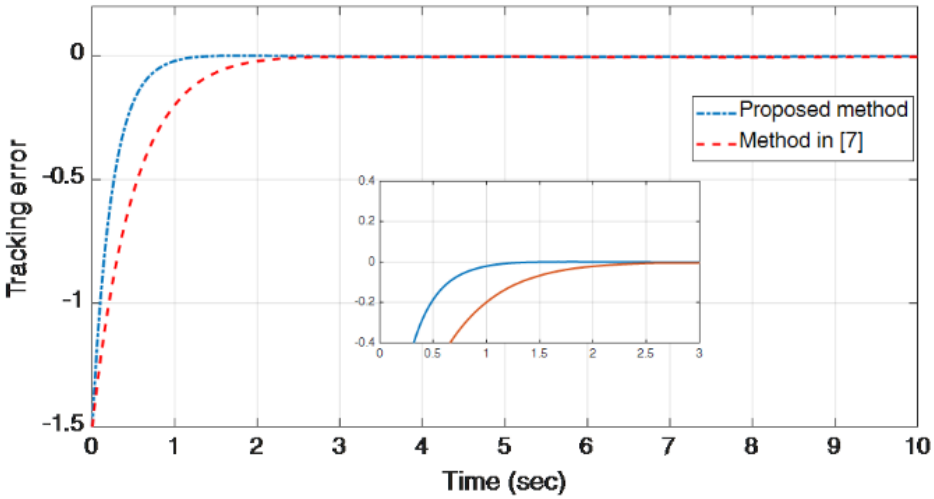

Fig. 6. Tracking errors.

(27), when the controller is activated, the errors of synchronization obtained are as those in Fig. 4. According to the simulation results, it is easy to observe that the master–slave systems are synchronized in finite-time.

In the following, we will compare the effectiveness of the designed controller (9) with the controller presented in [7]. Fig. 5 compares the output of the controller (9) and the controller presented in [7] with respect to the sine reference signal. Tracking errors are shown in Fig. 6. As it turns out, the controller presented in this article provides a faster response than the proposed controller in [7].

Remark 1: The sliding-mode control approach is a robust control method with many powerful characteristics, such as low sensitivity to external disturbances and robustness to the uncertainties due to structural variations and unmolded dynamics. Furthermore, the finite-time control strategies have demonstrated better robustness and disturbance rejection properties [61]. However, the TSMC law introduced in this paper can overcome time-varying parametric uncertainties and time-varying external disturbances.

5. CHAOS-BASED SECURE COMMUNICATION SCHEME

In the last section, the chaotic secure communication system by analog signal is also analyzed. The analog message signal

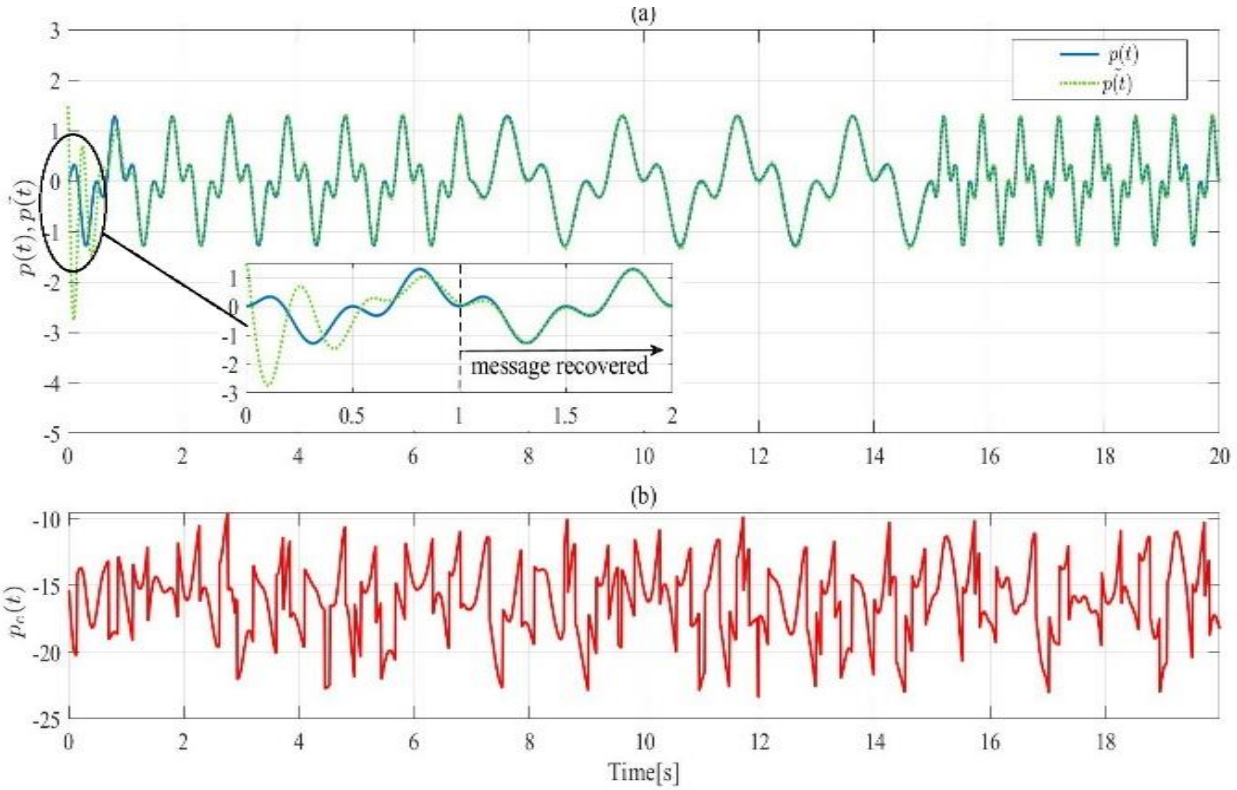

Fig. 7. Analog message, (a) original and recovered message signals, (b) encrypted message signal.

$p(t)$ is composed of a sequence of sine waves with frequencies $\omega = \pi, 2\pi$ and 3π $red/\sec$. In the real case, transmission channel adds the noise $n_d(t)$ to the transmitted signals. Therefore, in the simulations, transmitted signals are impregnated with the additive white Gaussian noise (AWGN). To clean the signals from the noise, a bank of filters is considered as the butter worth type at the input of the base station and mobile equipment [62]. The original and recovered message signals are illustrated in Fig. 15. In this figure, the top subfigures show the original message signal $p(t)$ and the reiterative message signal $\tilde{p}(t)$. The bottom subfigure shows the encrypted message signal $p_e(t)$ for the analog message, respectively. As it can be confirmed from these figures, the encrypted message signal is recovered in $t = 1s$ approximately.

6. CONCLUSIONS

A novel exponential 6D hyper–chaotic system was reported in this study. The dynamic behavior of the proposed system was analyzed. The new hyper–chaotic system had extremely complicated dynamics and structure. Next, a terminal sliding-mode controller was designed for stabilizing the new hyper–chaotic system with uncertainty and unknown disturbances. The results obtained from the fast terminal SMC were verified using the Lyapunov stability theory. A new controller was designed for finite-time synchronization between the two identical proposed hyper–chaotic systems in the presence of unequal parameters, different initial conditions and matched disturbances. The new controller feature was that the sliding surface designed with the high–order power function of error and the derivative of error was new and stable. Finally, the numerical simulations showed the viability of the designed methods. The simulations demonstrated that the analytical results and computational results are similar.

REFERENCES

[1] A. Alghafis, N. Munir, M. Khan, and I. Hussain, “An Encryption Scheme Based on Discrete Quantum Map and Continuous Chaotic System,” *International Journal of Theoretical Physics*, pp. 1-14, 2020.

[2] M. C. Pai, “Chaos control of uncertain time-delay chaotic systems with input dead-zone nonlinearity,” *Complexity*, vol. 21, no. 3, pp. 13-20, 2016.

[3] Z.-H. Guan, F. Huang, and W. Guan, “Chaos-based image encryption algorithm,” *Physics Letters A*, vol. 346, no. 1-3, pp. 153-157, 2005.

[4] R. Sedivy, and R. M. Mader, “Fractals, chaos, and cancer: do they coincide?,” *Cancer investigation*, vol. 15, no. 6, pp. 601-607, 1997.

[5] H. Gritli, “Robust master-slave synchronization of chaos in a one-sided 1-DoF impact mechanical oscillator subject to parametric uncertainties and disturbances,” *Mechanism and Machine Theory*, vol. 142, pp. 103610, 2019/12/01/, 2019.

[6] B. Xu, Y. Wang, and L. Liu, "Twice Pulse Ignition Boost Strategy for

missile guidance Based on Improved Particle Swarm Optimization Algorithm." pp. 9907-9912.

[7] M. P. Aghababa, "Stabilization of canonical systems via adaptive chattering free sliding modes with no singularity problems," *IEEE Transactions on Systems, Man, and Cybernetics: Systems*, 2018.

[8] M. Sciamanna, and K. A. Shore, "Physics and applications of laser diode chaos," *Nature photonics,* vol. 9, no. 3, pp. 151-162, 2015.

[9] K. Fallahi, and H. Leung, "A chaos secure communication scheme based on multiplication modulation," *Communications in Nonlinear Science and Numerical Simulation,* vol. 15, no. 2, pp. 368-383, 2010.

[10] C. Nwachioma, J. H. Pérez-Cruz, A. Jiménez, M. Ezuma, and R. Rivera-Blas, "A New Chaotic Oscillator—Properties, Analog Implementation, and Secure Communication Application," *IEEE Access,* vol. 7, pp. 7510-7521, 2019.

[11] K. Benkouider, T. Bouden, and M. E. Yalcin, "A snail-shaped chaotic system with large bandwidth: dynamical analysis, synchronization and secure communication scheme," *SN Applied Sciences,* vol. 2, pp. 1-15, 2020.

[12] Z.-A. S. A Rahman, H. A. Al-Kashoash, S. M. Ramadhan, and Y. I. Al-Yasir, "Adaptive Control Synchronization of a Novel Memristive Chaotic System for Secure Communication Applications," *Inventions,* vol. 4, no. 2, pp. 30, 2019.

[13] C. Xiu, R. Zhou, and Y. Liu, "New chaotic memristive cellular neural network and its application in secure communication system," *Chaos, Solitons & Fractals,* vol. 141, pp. 110316, 2020.

[14] F. Zhu, F. Wang, and L. Ye, "Artificial switched chaotic system used as transmitter in chaos-based secure communication," *Journal of the Franklin Institute,* 2020.

[15] J. Wang, W. Yu, J. Wang, Y. Zhao, J. Zhang, and D. Jiang, "A new six-dimensional hyperchaotic system and its secure communication circuit implementation," *International Journal of Circuit Theory and Applications,* vol. 47, no. 5, pp. 702-717, 2019.

[16] V. Afraimovich, N. Verichev, and M. I. Rabinovich, "Stochastic synchronization of oscillation in dissipative systems," *Radiophysics and Quantum Electronics,* vol. 29, no. 9, pp. 795-803, 1986.

[17] E. Ott, C. Grebogi, and J. A. Yorke, "Controlling chaos," *Physical review letters,* vol. 64, no. 11, pp. 1196, 1990.

[18] Z. Sun, L. Si, Z. Shang, and J. Lei, "Finite-time synchronization of chaotic PMSM systems for secure communication and parameters identification," *Optik,* vol. 157, pp. 43-55, 2018.

[19] W. Wang, X. Jia, X. Luo, J. Kurths, and M. Yuan, "Fixed-time synchronization control of memristive MAM neural networks with mixed delays and application in chaotic secure communication," *Chaos, Solitons & Fractals,* vol. 126, pp. 85-96, 2019.

[20] S. Khorashadizadeh, and M.-H. Majidi, "Chaos synchronization using the Fourier series expansion with application to secure communications," *AEU-International Journal of Electronics and Communications,* vol. 82, pp. 37-44, 2017.

[21] M. F. Hassan, and M. Hammuda, "A new approach for constrained chaos synchronization with application to secure data communication," *Journal of the Franklin Institute,* vol. 356, no. 12, pp. 6697-6723, 2019.

[22] Y.-J. Chen, H.-G. Chou, W.-J. Wang, S.-H. Tsai, K. Tanaka, H. O. Wang, and K.-C. Wang, "A polynomial-fuzzy-model-based synchronization methodology for the multi-scroll Chen chaotic secure communication system," *Engineering Applications of Artificial Intelligence,* vol. 87, pp. 103251, 2020.

[23] Q. Li, and C. Yue, "Predefined-time Polynomial-function-based Synchronization of Chaotic Systems Via a Novel Sliding Mode Control," *IEEE Access,* 2020.

[24] W. Yu, J. Wang, J. Wang, H. Zhu, M. Li, Y. Li, and D. Jiang, "Design of a new seven-dimensional hyperchaotic circuit and its application in secure communication," *IEEE Access,* vol. 7, pp. 125586-125608, 2019.

[25] F. Yu, Z. Zhang, L. Liu, H. Shen, Y. Huang, C. Shi, S. Cai, Y. Song, S. Du, and Q. Xu, "Secure communication scheme based on a new 5D multistable four-wing memristive hyperchaotic system with disturbance inputs," *Complexity,* vol. 2020, 2020.

[26] J. P. Singh, K. Lochan, and B. K. Roy, "Secure Communication Using a New Hyperchaotic System with Hidden Attractors," *Control Instrumentation Systems,* pp. 67-79: Springer, 2020.

[27] P. Trikha, and L. S. Jahanzaib, "Dynamical analysis of a novel 5-d hyper-chaotic system with no equilibrium point and its application in secure communication," *Differential Geometry--Dynamical Systems,* vol. 22, 2020.

[28] L. Yang, Q. Yang, and G. Chen, "Hidden attractors, singularly degenerate heteroclinic orbits, multistability and physical realization of a new 6D hyperchaotic system," *Communications in Nonlinear Science and Numerical Simulation,* pp. 105362, 2020.

[29] F. Yu, L. Liu, B. He, Y. Huang, C. Shi, S. Cai, Y. Song, S. Du, and Q. Wan, "Analysis and FPGA realization of a novel 5D hyperchaotic four-wing memristive system, active control synchronization, and secure communication application," *Complexity,* vol. 2019, 2019.

[30] W. Tai, Q. Teng, Y. Zhou, J. Zhou, and Z. Wang, "Chaos synchronization of stochastic reaction-diffusion time-delay neural networks via non-fragile output-feedback control," *Applied Mathematics and Computation,* vol. 354, pp. 115-127, 2019/08/01/, 2019.

[31] L. Wang, and M. Ding, "Dynamical analysis and passive control of a new 4D chaotic system with multiple attractors," *Modern Physics Letters B,* vol. 32, no. 22, pp. 1850260, 2018.

[32] K. Rajagopal, H. Jahanshahi, M. Varan,

I. Bayır, V.-T. Pham, S. Jafari, and A. Karthikeyan, "A hyperchaotic memristor oscillator with fuzzy based chaos control and LQR based chaos synchronization," *AEU-International Journal of Electronics and Communications,* vol. 94, pp. 55-68, 2018.

[33] H. Jahanshahi, A. Yousefpour, J. M. Munoz-Pacheco, I. Moroz, Z. Wei, and O. Castillo, "A new multi-stable fractional-order four-dimensional system with self-excited and hidden chaotic attractors: Dynamic analysis and adaptive synchronization using a novel fuzzy adaptive sliding mode control method," *Applied Soft Computing,* vol. 87, pp. 105943, 2020.

[34] M. M. Zirkohi, "Chaos synchronization using higher-order adaptive PID controller," *AEU-International Journal of Electronics and Communications,* vol. 94, pp. 157-167, 2018.

[35] S. Vaidyanathan, S. T. Kingni, A. Sambas, M. A. Mohamed, and M. Mamat, "A new chaotic jerk system with three nonlinearities and synchronization via adaptive backstepping control," *International Journal of Engineering & Technology,* vol. 7, no. 3, pp. 1936-1943, 2018.

[36] C. Huang, L. Cai, and J. Cao, "Linear control for synchronization of a fractional-order time-delayed chaotic financial system," *Chaos, Solitons & Fractals,* vol. 113, pp. 326-332, 2018.

[37] M.-H. Wang, S.-D. Lu, and M.-J. Hsieh, "Application of extension neural network algorithm and chaos synchronization detection method to partial discharge diagnosis of power capacitor," *Measurement,* vol. 129, pp. 227-235, 2018.

[38] A. Mohammadzadeh, S. Ghaemi, and O. Kaynak, "Robust predictive synchronization of uncertain fractional-order time-delayed chaotic systems," *Soft Computing,* vol. 23, no. 16, pp. 6883-6898, 2019.

[39] Y. Yin, F. Liu, and P. Shi, "Finite-time continuous gain-scheduled control on stochastic hyperchaotic systems," *Proceedings of the Institution of Mechanical Engineers, Part I: Journal of Systems and Control Engineering,* vol. 224, no. 6, pp. 679-688, 2010.

[40] E. D. Dongmo, K. S. Ojo, P. Woafo, and A. N. Njah, "Difference synchronization of identical and nonidentical chaotic and hyperchaotic systems of different orders using active backstepping design," *Journal of Computational and Nonlinear Dynamics,* vol. 13, no. 5, 2018.

[41] P. Muthukumar, P. Balasubramaniam, and K. Ratnavelu, "Sliding mode control design for synchronization of fractional order chaotic systems and its application to a new cryptosystem," *International Journal of Dynamics and Control,* vol. 5, no. 1, pp. 115-123, 2017.

[42] S. Vaidyanathan, L. G. Dolvis, K. Jacques, C.-H. Lien, and A. Sambas, "A new five-dimensional four-wing hyperchaotic system with hidden attractor, its electronic circuit realisation and synchronisation via integral sliding mode control," *International Journal of Modelling,*

Identification and Control, vol. 32, no. 1, pp. 30-45, 2019.

[43] X. Xi, S. Mobayen, H. Ren, and S. Jafari, "Robust finite-time synchronization of a class of chaotic systems via adaptive global sliding mode control," *Journal of Vibration and Control,* vol. 24, no. 17, pp. 3842-3854, 2018.

[44] A. Modiri, and S. Mobayen, "Adaptive terminal sliding mode control scheme for synchronization of fractional-order uncertain chaotic systems," *ISA Transactions*, 2020.

[45] X. Chang, L. Liu, W. Ding, D. Liang, C. Liu, H. Wang, and X. Zhao, "Novel nonsingular fast terminal sliding mode control for a PMSM chaotic system with extended state observer and tracking differentiator," *Journal of Vibration and Control,* vol. 23, no. 15, pp. 2478-2493, 2017.

[46] B. Mao, "Two methods for terminal sliding-mode synchronization of fractional-order nonlinear chaotic systems," *Asian Journal of Control*.

[47] F. Plestan, Y. Shtessel, V. Bregeault, and A. Poznyak, "New methodologies for adaptive sliding mode control," *International journal of control,* vol. 83, no. 9, pp. 1907-1919, 2010.

[48] M. Fu, S. Gao, C. Wang, and M. Li, "Human-centered automatic tracking system for underactuated hovercraft based on adaptive chattering-free full-order terminal sliding mode control," *IEEE Access,* vol. 6, pp. 37883-37892, 2018.

[49] Z. Song, C. Duan, J. Wang, and Q. Wu, "Chattering-free full-order recursive sliding mode control for finite-time attitude synchronization of rigid spacecraft," *Journal of the Franklin Institute,* vol. 356, no. 2, pp. 998-1020, 2019.

[50] L. Wan, G. Chen, M. Sheng, Y. Zhang, and Z. Zhang, "Adaptive chattering-free terminal sliding-mode control for full-order nonlinear system with unknown disturbances and model uncertainties," *International Journal of Advanced Robotic Systems,* vol. 17, no. 3, pp. 1729881420925295, 2020.

[51] X. Gao, and Y. Weng, "Chattering-free model free adaptive sliding mode control for gas collection process with data dropout," *Journal of Process Control,* vol. 93, pp. 1-13, 2020.

[52] P. A. Hosseinabadi, A. S. S. Abadi, S. Mekhilef, and H. R. Pota, "Chattering-free trajectory tracking robust predefined-time sliding mode control for a remotely operated vehicle," *Journal of Control, Automation and Electrical Systems*, pp. 1-19, 2020.

[53] J. Mei, Z. Lu, J. Hu, and Y. Fan, "Guaranteed Cost Finite-Time Control of Uncertain Coupled Neural Networks," *IEEE Transactions on Cybernetics*, 2020.

[54] S. Wiggins, *Introduction to applied nonlinear dynamical systems and chaos*: Springer Science & Business Media, 2003.

[55] E. E. Mahmoud, "Generation and suppression of a new hyperchaotic nonlinear model with complex variables," *Applied Mathematical Modelling,* vol. 38, no. 17-18, pp. 4445-4459, 2014.

[56] T. F. Fonzin, J. Kengne, and F. Pelap, "Dynamical analysis and multistability in autonomous hyperchaotic oscillator with experimental verification," *Nonlinear Dynamics,* vol. 93, no. 2, pp. 653-669, 2018.

[57] Z. Njitacke, J. Kengne, R. W. Tapche, and F. Pelap, "Uncertain destination dynamics of a novel memristive 4D autonomous system," *Chaos, Solitons & Fractals,* vol. 107, pp. 177-185, 2018.

[58] A. Wolf, J. B. Swift, H. L. Swinney, and J. A. Vastano, "Determining Lyapunov exponents from a time series," *Physica D: Nonlinear Phenomena,* vol. 16, no. 3, pp. 285-317, 1985.

[59] S. T. Tchinda, G. Mpame, A. N. Takougang, and V. K. Tamba, "Dynamic analysis of a snap oscillator based on a unique diode nonlinearity effect, offset boosting control and sliding mode control design for global chaos synchronization," *Journal of Control, Automation and Electrical Systems,* vol. 30, no. 6, pp. 970-984, 2019.

[60] A. Abdurahman, H. Jiang, and Z. Teng, "Finite-time synchronization for memristor-based neural networks with time-varying delays," *Neural Networks,* vol. 69, pp. 20-28, 2015.

[61] W. Yu, "Finite-time stabilization of three-dimensional chaotic systems based on CLF," *Physics Letters A,* vol. 374, no. 30, pp. 3021-3024, 2010.

[62] M. Z. De la Hoz, L. Acho, and Y. Vidal, "A modified Chua chaotic oscillator and its application to secure communications," *Applied Mathematics and Computation,* vol. 247, pp. 712-722, 2014..